CHEMISTRY OF MATERIALS

Article

pubs.acs.org/cm

Dual-Responsive Polymer Micelles for Target-Cell-Specific Anticancer Drug Delivery

Xing Guo,[†] Chunli Shi,[‡] Guang Yang,[†] Jie Wang,[†] Zhenghong Cai,[‡] and Shaobing Zhou*[,†,‡]

[†]Key Laboratory of Advanced Technologies of Materials, Ministry of Education, School of Materials Science and Engineering, [‡]School of Life Science and EngineeringSouthwest Jiaotong University, Chengdu 610031, China

Supporting Information

ABSTRACT: Efficient delivery of therapeutic agents with nanocarriers into the nucleus to achieve high therapeutic efficiency is still a major challenge for cancer therapy due to mucosal barriers, nonspecific uptake, and intracellular drug resistance. In this study, we develop a dual-responsive polymer micelle system with sheddable polyethylenimine (PEI) shells for actively targeted drug delivery. This system exhibits an ultrasensitive negative-to-positive charge reversal in response to the extracellular pH value, resulting in greatly enhanced uptake by cancer cells via electrostatic interaction. Moreover, the active targeting ability can further promote the selective uptake of the nanocarriers in the cancer cell. Once the micelles escape from the lysosomes, the disulfide linkages can be cleaved by GSH in the cytoplasm, and in turn the hydrophilic PEI shell is deshielded, leading to the rapid release of the encapsulated agent into the nuclei. The antitumor activity in 4T1 tumor-bearing mice reveals that this novel system possesses a long blood circulation due to the originally negatively charged surface and can significantly promote the cell internalization and intracellular drug release, thus leading to a high therapeutic efficacy against resistant tumors and fewer side effects to normal tissues.

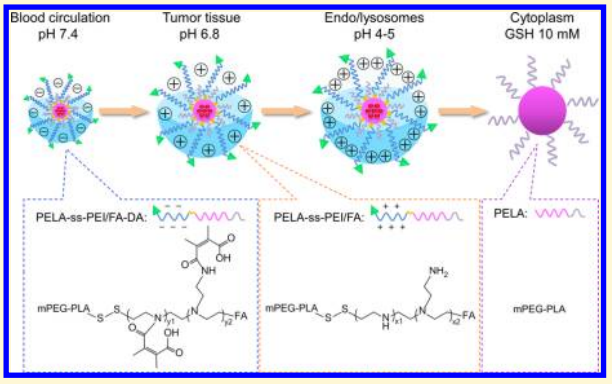

INTRODUCTION

Most anticancer drugs, such as doxorubicin (DOX) and cisplatin, are DNA toxins, which target nuclear DNA to cause DNA damage and/or inhibit topoisomerase to induce cell death.[1,2] They thus have to enter the nucleus for their pharmacological effects to be elicited. In an attempt to achieve an effective delivery of the therapeutics agent to target, nanoparticle (NP)-based drug delivery system has attracted more and more attention. From the injection site to the final nucleus, NPs have a long travel with various physiological and biological barriers, including circulating via blood to the tumor tissue, being internalized by the cancer cells, escaping the lysosomes, and finally releasing the drug to nucleus. As a result, only a small percentage of drugs reaches the nucleus after passing these barriers *in vivo*. Therefore, efficient delivery of a therapeutic agent with NPs into the tumor cell nucleus to achieve high therapeutic efficiency is still a major challenge for cancer therapy.

Although the accumulation of NPs in tumor tissues can be enhanced by the well-known enhanced permeation and retention (EPR) effect,[3,4] the safety and stability of NPs in the blood resulting from the surface chemistry of NPs, such as surface charge, are paramount considerations for *in vivo* application. NPs with a negatively charged surface are effective for protein resistance to possess a long blood circulation,[5] while positively charged NPs undergo substantial phagocytosis by the reticular endothelin system (RES) and interact strongly with serum components, causing severe aggregation and a short blood circulation half-life.[6] However, compared with the negatively charged NPs, positively charged NPs are expected to be more readily internalized by cancer cells since they have high affinity for negatively charged cell membranes. To solve this opposition, an ideal scenario would be that the positive charges of NPs are masked during the blood circulation but are regenerated once localized in the tumor tissue.

After the NPs pass through the first barrier in the blood and arrive in tumor tissue, the internalization of NPs by cancer cells becomes an urgent task. In addition to endowing the NPs a negative-to-positive charged surface, grafting NPs with various targeting ligands whose receptors are overexpressed on cancer cells is another effective strategy to enhance the internalization.[7] For instance, folate (FA), binding with high affinity to the folate receptor (FR), has been widely used to modify NPs to further improve the selective targeting to cancer cells.[8−11] Although the targeting ligands-attached NPs can significantly facilitate the cell internalization by receptor-mediated endocytosis, they will go on encountering compartments inside the cell, namely early endosomes, late endosomes, and lysosomes. Thus, it is still a challenging task to realize the intracellular drug release.

Received: April 9, 2014
Revised: July 21, 2014
Published: July 21, 2014

   dx.doi.org/10.1021/cm5012718 | *Chem. Mater.* 2014, 26, 4405−4418

Scheme 1. Schematic Design of the Targeted Micelles (PELE/DA-FA) with Charge Reversal to the Tumor Extracellular Matrix and Intracellular GSH-Triggered Drug Release

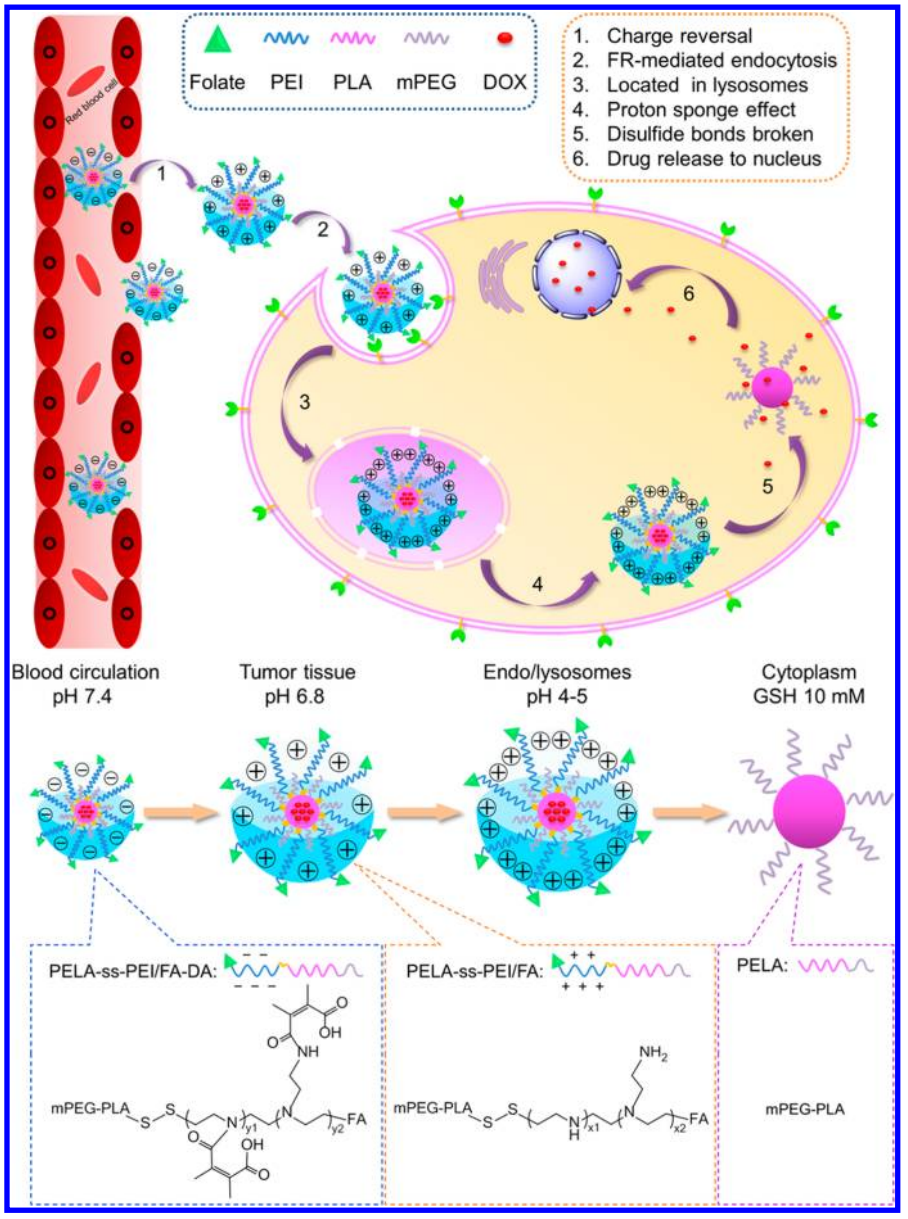

To address this challenge, stimuli-responsive delivery systems have been extensively investigated. Of these stimuli, pH-response is the most frequently used, as pH values vary in different tissues and cellular compartments.[12] Various pH-responsive drug delivery systems have been constructed for realizing the pH-triggered drug release.[13−15] Nevertheless, most of these systems are only responsive to a single pH variation, either in the tumor extracellular environment or in the intracellular endo/lysosomal condition. To overcome the limitations, pH-dependent charge reversal was recently utilized for NPs development for nuclear drug delivery.[16−18] The other interesting strategy to trigger drug release is by utilizing sheddable shells, in which shedding of the "stealth" NPs in response to a stimulus would result in destabilization of the NPs.[19] Among all of the applied stimuli, redox potential is a potent stimuli for NPs containing disulfide linkages, owing to the fact that the disulfide bonds can be cleaved by excess glutathione (GSH).[20−22]

Accordingly, in this study we develop a dual-responsive polymer micelle system with sheddable polyethylenimine (PEI) shells for actively targeted anticancer drug delivery. Micelles, which have a core/shell architecture and are used as drug carriers for loading poorly water-soluble drugs, are usually associated with several advantages, including enhanced drug solubility in water, prolonged blood circulation, EPR effect, decreased side effects, and improved drug bioavailability.[23−25] In this micelle system, PEI has been extensively explored for gene and drug delivery. It can promote the entry of materials into the nucleus.[26−28] The primary and secondary amines of the PEI block are converted into amides with neighboring carboxylic acid groups, which display pH-dependent hydrolysis and subsequently achieve a negative-to-positive charge reversal under different pH conditions.[29,30] As shown in Scheme 1, the polymer micelles that are negatively charged under neutral conditions can maintain their stability and prolong the circulation time in blood. Once accumulated at the tumor

dx.doi.org/10.1021/cm5012718 | Chem. Mater. 2014, 26, 4405−4418

site by the EPR effect, they can be internalized both through an electrostatic interaction due to the negative-to-positive charge reversal in response to the tumor extracellular pH and by FR-mediated endocytosis, escape from lysosomes via a proton sponge effect, deshield the PEI shells by excess intracellular GSH, and release the drug to nucleus. The development of folate targeting and dual-responsive micelle system and usage in both *in vitro* and *in vivo* have been rarely reported, and thus provide a novel and versatile approach for efficient cancer chemotherapy.

MATERIALS AND METHODS

Materials. Poly(ethylenimine), 2,3-dimethylmaleic anhydride (DMMA), 3,3′-dithiodipropionic acid (DTDP) and glutathione (GSH) were purchased from Adamas-beta. Methoxy polyethylene glycol (mPEG, M_w = 750) was purchased from Alfa Aesar. D, L-Lactide was prepared in our own laboratory. Succinic anhydride (SA) and folate (FA) were purchased from Chengdu KeLong Chemical Reagent Company (Sichuan, China). Doxorubicin hydrochloride (DOX·HCl) was purchased from Zhejiang Hisun Pharmaceutical Co., Ltd. (China). All the other chemicals were purchased from commercial suppliers and used without further purification.

Cell Lines and Culture Conditions. The human cervix adenocarcinoma cell line HeLa (FR positive), human lung epithelial carcinoma cell line A549 (FR negative), mouse fibroblast cell line NIH 3T3, and mouse mammary tumor cell line 4T1 (FR negative) were obtained from Sichuan University (China). Cells were cultured in RPMI 1640 added with 10% fetal bovine serum (FBS) at 37 °C in an atmosphere of 5% CO_2 and 95% air under fully humidified conditions. To upregulate FR expression of FR-negative 4T1 cells, a very low level (10 pmol/L) of folate was added in growth medium of 4T1 cells for continuous culturing.[31] All of the 4T1 cells mentioned in following *in vitro* cellular uptake and cytotoxicity and mouse xenograft tumor models were FR-upregulated 4T1 cells.

Animals. Male BALB/c mice and nude mice (20 ± 2 g), used at 5−6 weeks of age, were approved by the Institutional Animal Care and Use Committee of Sichuan University and fed under conditions of 25 °C and 55% of humidity. All animals received care in compliance with the guidelines.

Preparation of Blank and DOX-Loaded Micelles. The blank micelles were prepared by using a solvent evaporation method. For instance, 10 mg of freeze-dried PELE/FA-DA powder was dissolved in 5 mL of tetrahydrofuran (THF); the solution was then added dropwise into 10 mL of deionized water by using a disposable syringe (21 gauge) under high-speed stirring. The micelles gradually formed with the evaporation of THF. To prepare the DOX-loaded micelles, 1 mg of DOX·HCl was dissolved in 5 mL of THF, and then a drop of TEA was added and reacted with DOX·HCl for 1 h to remove the hydrochloric acid. Afterward, 10 mg of freeze-dried PELE/FA-DA powder was added to the DOX solution, with the following step similar to that above. After THF was completely evaporated, the micellar solution was dialyzed against demonized water to remove the unloaded drug. The drug-loaded micelles were collected by lyophilization. The fabrication of the other blank and DOX-loaded micelles underwent similar processes.

Characterization of Terpolymer. ^{1}H Nuclear magnetic resonance (^{1}H NMR) spectra were obtained on a Bruker AM 300 apparatus. $CDCl_3$, DMSO-d_6 or D_2O was used as a solvent, and tetramethylsilane (TMS) was used as the internal reference. Chemical shifts are expressed in parts per million, ppm (δ). The full ultraviolet spectrum of PELE/FA-DA terpolymer was measured with a UV−vis spectrophotometer (UV-2550, Shimadzu, Japan) to confirm the successful graft of folate and quantify the grafted amount. The molecular weights of the terpolymers were analyzed using a gel permeation chromatography (GPC) system consisting of a Waters 2695 pump and a Styragel HT4DMF column. DMF was used as the eluent at a flow rate of 1 mL/min at 40 °C, and the molecular weights were calibrated with polystyrene as standards.

Characterization of Micelles. The critical micelle concentration (CMC) of PELE/FA-DA micelle was determined by a fluorescence spectrophotometer (F-7000, Hitach, Japan). Pyrene was used as a fluorescent probe. The excitation wavelength was set to 333 or 339 nm, and the fluorescence intensity was detected at 372 nm. CMC was estimated as the cross-point when extrapolating the intensity ratio I_{339}/I_{333} at low and high concentration regions. The average size and ζ potential of micelles were determined by dynamic light scattering (DLS) (Zeta-Sizer, Malvern Nano-ZS90, Malvern, U.K.) at 25 °C. Each measurement was carried out in triplicate, and an average value was reported. The morphologies of micelles were tested by transmission electron microscopy (TEM) performed with a JEOL 2010F instrument (JEOL Ltd., Japan) operated at 200 kV. Samples were prepared by drying a drop of the micellar solution (1 mg/mL) on a copper grid coated with amorphous carbon. Afterward, a drop of phosphotungstic acid solution (1%) was added to the copper grid to stain the micelles, 1 min later, a filter paper was performed to absorb the solution. The grid was completely dried before TEM observation. DOX-loading content (LC) and encapsulation efficiency (EE) were analyzed by UV−vis spectrophotometer. The freeze-dried sample was weighed and redissolved in DMSO. The absorbance of DOX at 488 nm was measured to quantify the DOX concentration in the solution using a pre-established calibration curve.

Characterization of Protein Adsorption by Micelles. The PELE, PELE-SA, and PELE/FA-DA micelles were mildly mixed with 0.25 mg/mL bovine serum albumin (BSA) (Sigma-Aldrich) solution in phosphate buffered saline (PBS). The average size of micelles after different periods of incubation was determined by DLS at 25 °C.

Dual Responsive Behaviors. ^{1}H NMR was used to analyze the cleavage of the amide bonds formed between PEI and DMMA or SA, and GPC was used to detect the breakage of the disulfide bond in PELE/FA-DA. For ^{1}H NMR detection, PELE/FA-DA was dissolved in D_2O, and DCl was used to adjust pD to 6.8. The ^{1}H NMR spectra of the sample were recorded at 0, 10, 20, and 30 min. For GPC detection, PELE/FA-DA was incubated with 10 mM GSH for 24 h and dialyzed to remove GSH. The solution was collected and freeze-dried. The lyophilized sample was redissolved in DMF for GPC test. To measure the ζ potential and size change of the PELE/FA-DA and PELE-SA micelles at different pH values, the terpolymers were dissolved in PBS at pH 7.4 or 6.8 or acetate buffered solution (ABS) at pH 5.0, respectively. DLS was performed to detect the ζ potential and size of micelles at different time points. The size change of PELE/FA-DA micelles in response to different concentrations of GSH was measured by DLS. Ten μM or 10 mM GSH was incubated with 2 mL of micellar solution. The size of micelles was recorded at different time intervals. Fluorescence spectrophotometry was used to further analyze the reduction sensitivity of PELE/FA-DA micelles. Pyrene was used as a fluorescent probe. Briefly, 10 μM, 0.1 mM, 1 mM or 10 mM GSH was incubated with 2 mL of micellar solution. The excitation wavelength was set to 333 or 339 nm, and the fluorescence intensity was detected at 372 nm at different time points. The ratios of the peak intensities at 339 and 333 nm (I_{339}/I_{333}) of the excitation spectra were recorded. To directly observe the morphologies of micellar solution as a function of acidic pH and GSH, 10 mM GSH was incubated with PELE/FA-DA micelles at pH 5.0 for 24 h. TEM observation was performed after sample preparation. The buffering capacity of PELE/FA-DA was tested by acid−base titration over a pH range from 2.0 to 11.0. Briefly, the sample was dissolved in 0.1 M NaCl aqueous solution to reach a concentration of 2 mg/mL. Then 1 M NaOH was used to adjust the solution pH to 11.0, and titrated with 0.1 M HCl. PEI was used as the control sample.

***In Vitro* DOX Release.** In the direct measurement of DOX fluorescence intensity, a fluorescence spectrophotometer was used to analyze the release of DOX from PELE/FA-DA micelles as a function of pH and/or GSH. For pH sensitivity, 10 mg of DOX-loaded PELE/FA-DA freeze-dried powder was resuspended in 10 mL of PBS at pH 7.4 or ABS at pH 5.0, respectively. The samples were kept at 37 °C in a thermostated incubator with a shaking speed at 100 cycles/min. The intensity of DOX fluorescence emission at 595 nm was measured by fluorescence spectrophotometer at different time points. For reduction

sensitivity, certain amounts of GSH were added into the micellar solution to cause the final GSH concentrations to be 1, 5, and 10 mM, respectively. The DOX fluorescence was measured after 2 h. For dual sensitivity, 10 μM or 10 mM GSH was incubated with micellar solutions at pH 7.4 or 5.0, the drug fluorescence intensity was recorded at 0 and 2 h. To quantify the release rate of DOX from micelles, 10 mg of DOX-loaded PELE/FA-DA freeze-dried powder was resuspended in 10 mL of PBS at pH 7.4 or ABS at pH 5.0, GSH was added or not to cause the final concentrations to be 10 μM or 10 mM. The solutions were dialyzed against 20 mL of PBS or ABS with GSH or not under a predetermined sink condition. The samples were kept at 37 °C in a thermostated incubator with a shaking speed at 100 cycles/min. One mL of solution outside the dialysis bag was removed for fluorescence spectrophotometer detection and replaced with 1 mL of fresh medium at selected time intervals from 0.5 to 48 h. DOX concentration was calculated on the basis of the emission intensity of DOX at 595 nm. The cumulative amount of released DOX from micelles was calculated, and the percentages of released drug were plotted against time.

FR Surface Expression. FR surface expression of 4T1 cells, FR-upregulated 4T1 cells, and HeLa cells was evaluated by indirect immunostaining[32] using the antifolate binding protein antibody (Abcam (Hong Kong) Ltd., Abcam, HK, China) followed by Alexa Fluor 488 conjugated antirabbit secondary antibody (Bioss, Beijing, China). Nonspecific fluorescence was assessed using the secondary antibody only. Flow cytometric analyses were performed using a FACSCalibur flow cytometer (BD Biosciences, U.S.A.).

Cytocompatibility Assay. To evaluate the cytocompatibility of the blank micelles, both Alarmar Blue (AB) assay and live/dead staining were performed. For AB assay, 3T3 cells, HeLa cells, and 4T1 cells were plated at 2×10^4 per well in RPMI 1640 supplemented with 10% FBS. The next day, the cells were treated with blank micelles ranged from 10 μg/mL to 500 μg/mL at pH 7.4 or 6.8. The medium was removed 24 h later, the cells were washed three times with PBS, and 300 μL of AB solution (10% Alamar Blue, 80% media 199 (Gibcos) and 10% FBS, v/v) were added for a further 3 h of incubation. The solution of AB was then transferred into a 96-well plate, and the plate was read by an automated microplate spectrophotometer (ELX800 Biotek, U.S.A.) at 570 nm. For live/dead staining, 3T3 cells were seeded at a density of 1×10^4 cells per well for 24 h and treated with different concentrations of blank micelles at pH 7.4 or 6.8 for another day, the medium was removed, and each well was rinsed with PBS. Then the cells were stained with 2 mM calcein acetoxymethyl ester (Calcein-AM) for 10 min and 4 mM propidium iodide (PI) for 10 min in supplemented PBS. When observed using fluorescence microscopy, live cells were stained green and dead cells were stained red.

***In Vitro* Cellular Uptake and Subcellular Localization.** To evaluate the pH-sensitive cellular uptake of various DOX formulations, A549 cells were seeded in 6-well plates at a density of 10×10^4 cells/well and incubated for 24 h. Then the cells were treated with free DOX, DOX-loaded PECL, PELE, PELE-DA, and PELE/FA-DA micelles at pH 7.4 or 6.8, respectively. After incubation for 3 h at 37 °C, A549 cells were washed three times with PBS and fixed with fresh 2.5% glutaraldehyde for 30 min. The cells were then stained with 4′,6-diamidino-2-phenylindole (DAPI) for 5 min. The DAPI fluorescence (blue) and DOX fluorescence (red) inside the A549 cells were examined by an inverted fluorescence microscope (Olympus, CKX41) with a charge-coupled device camera (Imaging, Micropublisher 5.0 RTV) and a mercury lamp (Olympus, U-RFLT50). Confocal laser scanning microscopy (CLSM) was performed to observe the charge reversal internalization and subcellular distribution of DOX formulations. For charge reversal internalization, HeLa cells were seeded at a density of 10×10^4 cells/well into a confocal dish with RPMI 1640 and treated with DOX-loaded PELE or PELE-DA micelles at pH 7.4 or 6.8 24 h later. After incubation for 1 h at 37 °C, HeLa cells were washed with PBS, stained with Hoechst 33342 and Lysotracker Green (Beyotime Biotech, China) for cell nuclei and lysosomes, respectively. The cells were then observed on a confocal microscope (Olympus FV1000). For subcellular distribution observation, HeLa cells were treated with free DOX, DOX-loaded PECL, PELE-DA, and PELE/FA-DA micelles at pH 6.8. After incubation for 3 h, the cells were washed with PBS, stained with Hoechst 33342 and Lysotracker Green, and observed by CLSM. 4T1 cells were used for further investigation of charge reversal and FR-mediated endocytosis of micelles. The cells seeded at a density of 10×10^4 cells/well were treated with DOX-loaded PELE-DA and PELE-SA micelles at pH 7.4 or 6.8, and PELE/FA-DA or PELE/FA-DA micelles with a blocking dose of free folate (1 mM) at pH 7.4 for 1 h. Then, the cells were rinsed, stained with Lysotracker Green, and observed on a Leica Microsystems CMS Gmbh (TCS SP5, Germany). To observe the cellular uptake and drug release process in 4T1 cells, the cells were incubated with DOX-loaded PELE/FA-DA micelles at pH 6.8 for 1 h, 3, and 6 h, followed by rinsing, fixing, staining with DAPI and CLSM observation. The DOX concentration of free DOX and DOX-loaded micelles treated for all the three cells was 5 μg/mL.

Flow Cytometry. Flow cytometry was performed to quantitatively investigate the pH-sensitive celluar uptake and FR-mediated endocytosis of various DOX-loaded micelles. Briefly, HeLa cells (10×10^4 cells/well) grown in 6-well plates for 24 h were incubated with free DOX, DOX-loaded PECL, PELE, PELE-DA, and PELE/FA-DA micelles at pH 7.4 or 6.8 for 3 h. After that, cells were washed three times in PBS, trypsinized, centrifuged (1500 rpm, 5 min), and resuspended in PBS. DOX-positive cells were enumerated by FACSCalibur flow cytometer. 4T1 cells were used for flow cytometry analysis as well. The cells seeded at a density of 10×10^4 cells/well were treated with DOX-loaded PELE-DA and PELE-SA micelles at pH 7.4 or 6.8, and PELE/FA-DA or PELE/FA-DA micelles with a blocking dose of free folate (1 mM) at pH 7.4 for 1 h. Then, the cells were rinsed with PBS, trypsinized, collected, and resuspended in PBS for flow cytometric analyses.

The Effect of pH Value on Cytotoxicity. The cytotoxicity of various DOX formulations against HeLa cells and 4T1 cells at different pH conditions was also evaluated by AB assay. Two $\times 10^4$ cells were seeded in 48-well plates and incubated for 24 h. Then, the original medium of HeLa cells was replaced with different concentrations of free DOX, DOX-loaded PECL, PELE-DA, and PELE/FA-DA micelles containing DMEM of pH 7.4 or 6.8, respectively. For 4T1 cells, DOX-loaded PELE-DA micelles of pH 7.4 or 6.8, and PELE/FA-DA or PELE/FA-DA micelles with a blocking dose of free folate (1 mM) of pH 7.4 were replaced with the original medium for further incubation (DOX-equivalent dose: 10 μg/mL). After culturing for 24 h, the cells were washed with PBS, incubated with 300 μL of AB solution for further 3 h, and detected by amicroplate spectrophotometer.

Tumor Model. Male Balb/c mice, 5−6 weeks old, and nude mice (20 ± 2 g) were housed in groups of 4 with free access to water and kept at a temperature of 21 °C and relative humidity of 45−65%. Animals were acclimatized to the environment for at least 7 days before performing the procedures. All animal procedures were performed in compliance with the Institutional Animal Care and Use Committee of Sichuan University. 4T1 breast cancer was established by subcutaneous injection of 1×10^6 murine breast cancer 4T1 cells into the right lower leg. The tumor volume was calculated by the following equation: volume = $0.5 \times a \times b^2$, where a and b are width and length of the tumor, respectively.

***In Vivo* and *ex Vivo* DOX Fluorescence Imaging.** To directly observe the accumulation of various DOX formulations at tumor tissues, *in vivo* imaging was performed. Free DOX, DOX-loaded PELE, PELE-DA and PELE/FA-DA micelles were injected into 4T1 tumor-bearing nude mice via the lateral tail vein at a dosage of 5 mg DOX/kg body weight. The mice were then anesthetized and imaged by Maestro In-vivo Imaging System at 1 h, 6, and 24 h. At 24 h postinjection, the mice were sacrificed, and heart, liver, spleen, lung, kidney, and tumor were excised to directly observe the DOX fluorescence distribution. The emission fluorescence was collected from 500 to 750 nm, and the 455 nm excitation filter was used.

Pharmacokinetics and Biodistribution *in Vivo*. The quantitative amount of various formulations distributed in blood and tissues was estimated by the fluorescence measurement. Free DOX, DOX-loaded PELE, PELE-DA, and PELE/FA-DA micelles were adminis-

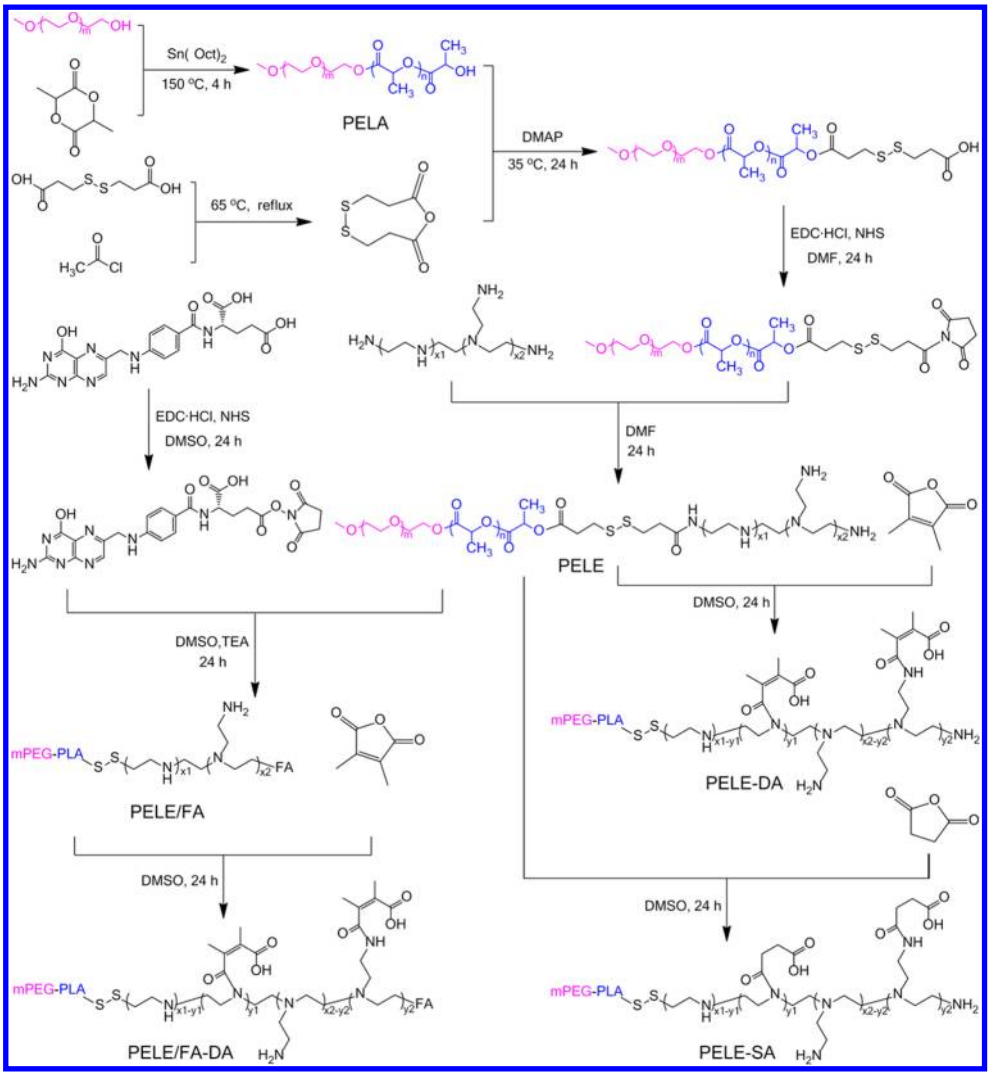

Figure 1. Synthesis of the targeted charge-reversal and reductive-sensitive copolymer PELE/DA-FA.

tered via the lateral tail vein at a dosage of 5 mg DOX/kg. Blood samples were obtained via eyeball extirpating at selected time intervals from 0.25 to 24 h using a heparinized capillary tube. The samples were then dissolved in lysis buffer (Beyotime Biotech, China), blended, and centrifuged at 12,000 rpm for 10 min to collect the supernatant. After blood collection, mice were sacrificed; the normal tissues including liver, heart, spleen, lung, kidney, and tumor were collected, washed with saline and weighed after drying. Then each tissue taken from the mice was dispersed in the lysis buffer and homogenized. The lysate of each tissue was centrifuged, and the supernatant was collected. The fluorescence intensity of the blood and tissue supernatant were measured by fluorescence spectrophotometer. Pharmacokinetic parameters such as $\tau_{1/2}$, area under the curve (AUC), volume of distribution (V_d) and clearance (CL) were calculated by fitting the blood drug pharmaceutical concentrations to a two-compartment model using EXCEL.[33,34] The percent injected dose (% ID) and the percent ID per gram (% ID/g) values were calculated using the following equations:

$$\%\mathrm{ID} = \frac{\text{dose in blood/tissue sample}}{\text{injected dose}} \times 100 \quad (1)$$

$$\%\mathrm{ID/g} = \frac{\%\mathrm{ID}}{\text{weight of tissue (g)}} \quad (2)$$

***In Vivo* Antitumor Effect.** 4T1-bearing Balb/c mice were randomly divided into six groups (seven mice per group). When the tumor volume of mice reached a mean size of about 50 mm^3, the treatments were carried out (this day was designated as "day 0"). Free DOX, DOX-loaded PELE, PELE-DA, and PELE/FA-DA micelles suspended in 100 μL of 0.9% NaCl solution were injected into mice via tail vein at an interval of 2 days (0, 3, 6, 9 day) at a dosage of 5 mg DOX/kg body weight. The same concentrations of PELE/FA-DA blank micelles were treated as well, and saline was used in control experiments. The tumor size and body weight were measured every 2 days, and the survival mice were monitored throughout the experiment.

Histological Analysis. For the histological analysis, the tumor tissue was isolated from the mice, fixed in 10% formalin and embedded in paraffin. Then the embedded specimens were sectioned and stained with hematoxylin and eosin (H&E).

***In Situ* Terminal Deoxynucleotidyltransferase-Mediated UTP End Labeling (TUNEL) Assay.** For TUNEL assay, the dewaxed and rehydrated tumor tissue sections were incubated with proteinase K for 20 min at RT, washed three times with saline, and the TUNEL assay in situ cell death detection kit (Roche Diagnostics GmbH, Mannheim, Germany) was used to detect apoptotic cells.

Statistical Analysis. SPSS software was used for the statistical data analysis. Data were expressed as means ± SD. One way ANOVA was performed to determine statistical significance of the data. The differences were considered significant for p values * < 0.05, # < 0.01 and ^ < 0.001, respectively.

dx.doi.org/10.1021/cm5012718 | *Chem. Mater.* 2014, 26, 4405−4418

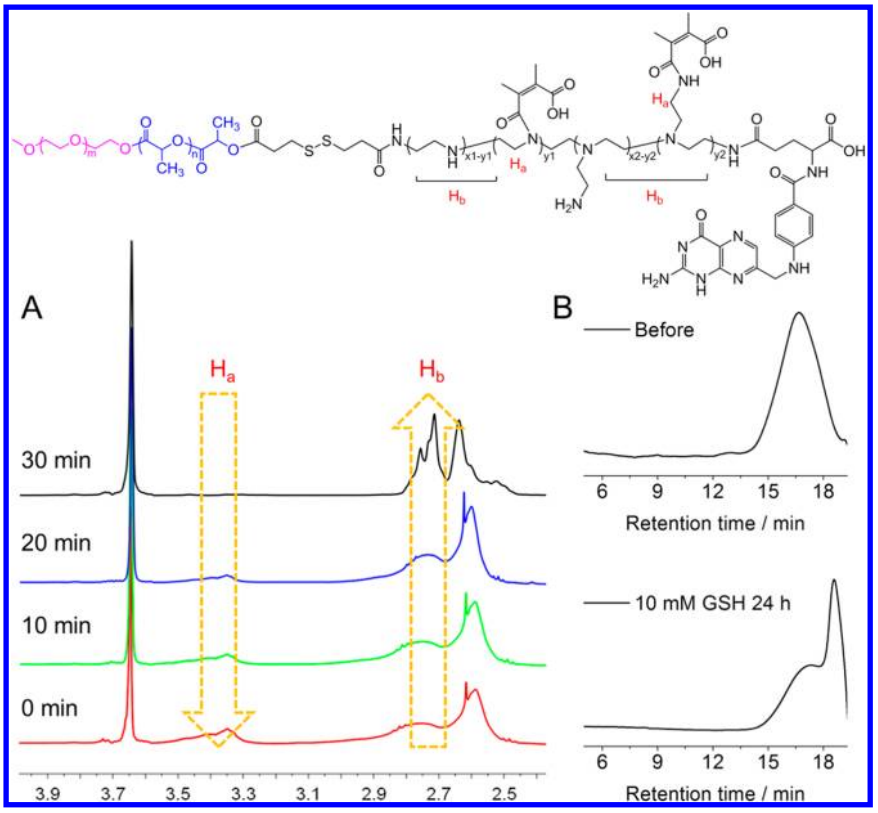

Figure 2. (A) ^{1}H NMR spectra of PELE/FA-DA after incubation at pD 6.8 in D_2O/DCl (25 °C) for different time periods. (B) GPC curves of disulfide bond broken in PELE/FA-DA before and under 10 mM GSH in DMF.

■ RESULTS AND DISCUSSION

Preparation and Characterization of PELE/FA-DA. To obtain the multifunctional polymer as NPs with active targeting ability to tumor site, tumor-activated charge-conversional capability and reductive-sensitivity to the extracellular and intracellular microenvironments of cancer cell, mPEG−PLA-ss-PEI/FA-DMMA (PELE/FA-DA) terpolymer was synthesized. As shown in Figure 1, mPEG−PLA (PELA) diblock copolymer was first synthesized from methoxy polyethylene glycol (mPEG) and D, L-lactide (LA) by ring-opening polymerization. The average degree of polymerization of PLA segment was 72, which was calculated on the basis of ^{1}H NMR analysis (Figure S1 in the Supporting Information (SI)). The terpolymer mPEG−PLA-ss-PEI (PELE) was then synthesized via the reaction of mPEG−PLA-ss-COOH (PELA-ss-COOH) with PEI, and the extent of PEI conjugation was about 100% according to ^{1}H NMR analysis (Figure S4 in SI). The PELE was further reacted with folate (FA) and 2,3-dimethylmaleic anhydride (DMMA) to obtain the PELE/FA-DA. As a control, succinic anhydride (SA) was reacted with PELE to obtain mPEG−PLA-ss-PEI-SA (PELE-SA) which possesses pH-stable amide bonds, and mPEG−PCL (PECL) with the same hydrophilic/hydrophobic ratio with PELE, lack of targeted ligand or environmental sensitivity, was synthesized as well. The number of conjugated DMMA or SA was 8.5 for PELE/FA-DA and 8 for PELE-SA on the basis of the calculation of ^{1}H NMR analysis (Figure S6 and Figure S8A in SI). Details of the characterizations are given in the SI (Figures S1−S8A).

^{1}H NMR of the PELE/FA-DA with a solvent of D_2O was performed to prove the core−shell structure of micelles (Figure S8B in SI). Compared to the ^{1}H NMR with DMSO-d_6 as solvent (Figure S8A in SI), the characteristic peaks of hydrophobic PLA block in D_2O almost disappeared, and those of FA, PEI, and mPEG still remained. The result strongly indicates that the PELE/FA-DA terpolymer successfully self-assembled into the well-defined core/shell structure micelles in aqueous solution. Besides, the FA ligand exposed outside of the shell can be utilized to recognize the folate receptors (FRs) on the cancer cells.

The average number of the attached FA molecules was calculated to be 0.5 per chain from the integration intensities of the aromatic protons in FA in the ^{1}H NMR (Figure S8A in SI). The molecular weight (M_n) of mPEG, PLA, and PEI block in PELE calculated from ^{1}H NMR analysis is 750, 5200, and 1700, respectively (Figure S4 in SI). In addition, Table S1 in SI summarizes the M_n of PELE, PELE-SA, PELE-DA, and PELE/FA-DA calculated by ^{1}H NMR, as well as the M_n and polydispersity (PDI) of these terpolymers detected by GPC.

The critical micelle concentration (CMC) value of PELE/FA-DA micelles was 3.048×10^{-3} mg/mL (Figure S9 in SI). Such a low CMC value ensures that the micelles could keep stable even if diluted within the body. The characterizations of micelles including Z-average diameters, PDI, drug loading content (LC), and drug encapsulation efficiency (EE) are summarized in Table S2 in SI. The three micelles decorated by anhydride showed higher EE (more than 60%) relative to that of the PELE micelles (27.06%). This high EE may be attributed to the interaction of negatively charged anhydride-decorated micelles with positively charged DOX. In contrast, the repulsive force between the positively charged PELE micelles and DOX may hamper drug loading.

Characterization of Protein Adsorption by Micelles. Negatively charged NPs can resist protein adsorption, while positively charged NPs are expected to have a high nonspecific

dx.doi.org/10.1021/cm5012718 | Chem. Mater. 2014, 26, 4405−4418

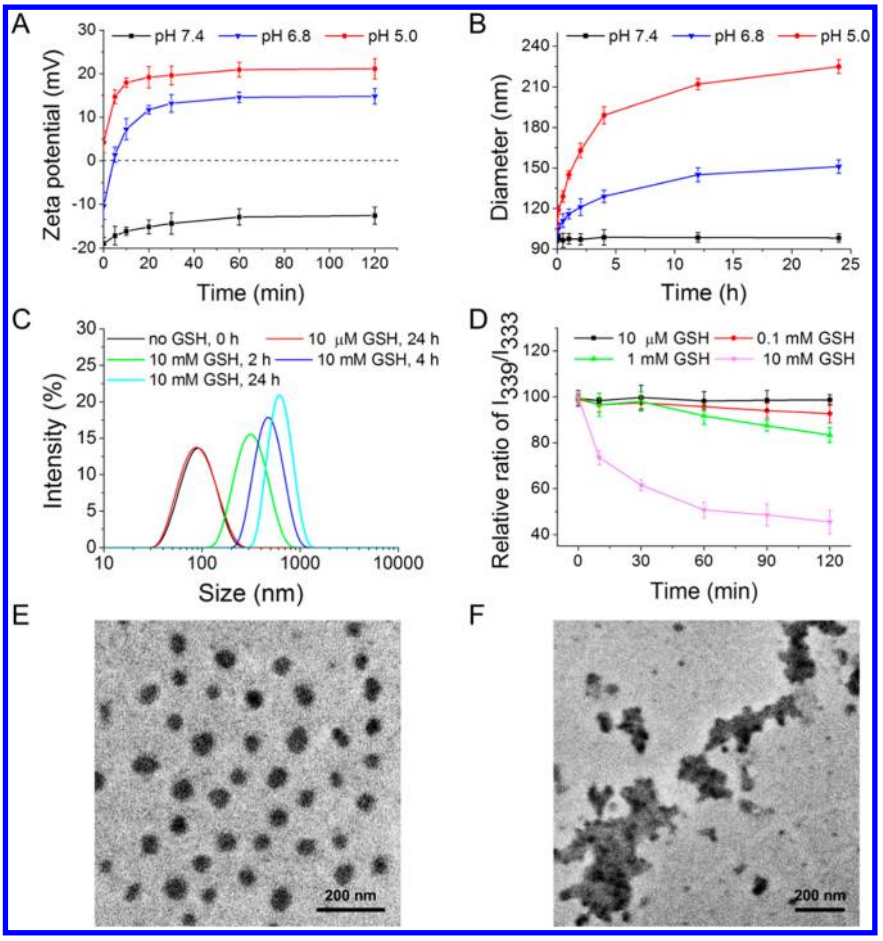

Figure 3. (A) ζ-Potential and (B) size change in PELE/FA-DA micelles as a function of incubation time at different pH values determined by DLS measurement. (C) The size change of PELE/FA-DA micelles in response to different concentrations of GSH. (D) The I_{339}/I_{333} ratio versus time determined by fluorescence spectrometer. Data are shown as mean ± SD (n = 3). Transmission electron microscopy (TEM) images of the PELE/DA-FA micelles at pH 7.4 (E) and pH 5.0 (F) with addition of 10 mM GSH.

internalization rate.[5,6,35] To demonstrate this, PELE, PELE-SA, and PELE/FA-DA micelles were incubated with 0.25 mg/mL bovine serum albumin (BSA) solution in phosphate buffered saline (PBS), and the average size of micelles against time were determined by dynamic light scattering (DLS) at 25 °C. The sizes of negatively charged PELE-SA and PELE/FA-DA micelles were slightly increased over time, while the size of positively charged PELE micelles significantly increased in a short time (Figure S10 in the SI). This phenomenon indicated that the protein adsorption of PELE micelles can be reduced by introducing negatively charged groups to the surface.

Dual Responsive Behaviors. Previous studies have proved that the amide bond formed between an amino and DMMA is cleavable under slightly acidic conditions.[17,36] To verify the acid-responsive cleavage of the amide bond in this study, we incubated PELE/FA-DA polymer at pD 6.8 and detected its ^{1}H NMR spectra at 0, 10, 20, and 30 min, and PELE-SA with pH stable amide bonds was used as a control. As shown in Figure 2A, the intensity of the peak of H_a decreased with the incubation and completely disappeared at 30 min, while that of H_b gradually increased, indicating the rapid acid-responsive cleavage of the amide bonds in PELE/FA-DA. However, the intensities of the peaks of both H_a and H_b remained unchanged at all tested times in PELE-SA (Figure S11 in SI). To prove the reductive sensitivity of PELE/FA-DA polymer, the change of molecular weight was measured, as determined by GPC in Figure 2B. Compared to the GPC curve of PELE/FA-DA without treating, a new peak occurred after it was preincubated with 10 mM GSH for 24 h, which was regarded as the peak of PEI released from PELE/FA-DA when the disulfide bond was cleaved.

Each amide bond in PELE/FA-DA polymer has a carboxyl group, thus the PELE/FA-DA micelles should be negatively charged at pH 7.4, and gradually become positively charged when the amide bonds hydrolyze to produce the primary amines or secondary amines of PEI in acidic environment. To confirm the charge reversal of PELE/FA-DA micelles, the ζ-potentials of the micellar solution were measured as shown in Figure 3A. PELE/FA-DA micelles revealed a ζ-potential of about −13 mV at pH 7.4 after incubation for 2 h, indicating that they were always negatively charged as a result of the presence of carboxyl groups. The value increased significantly when the micelles were incubated at pH 6.8, and kept constant 30 min later, which was in line with the result detected by ^{1}H NMR (Figure 2A). At pH 5.0, they immediately became positively charged and gradually reached a ζ-potential of about +21 mV. Therefore, the PELE/FA-DA micelles indeed showed charge-reversal behavior: they were always negatively charged at physiological pH, once localized in acidic microenvironment close to the pH value of solid tumors or endo/lysosomes, they hydrolyzed and became positively charged. The charge-reversal capability is obviously pH-dependent. In contrast, no sign of

dx.doi.org/10.1021/cm5012718 | Chem. Mater. 2014, 26, 4405−4418

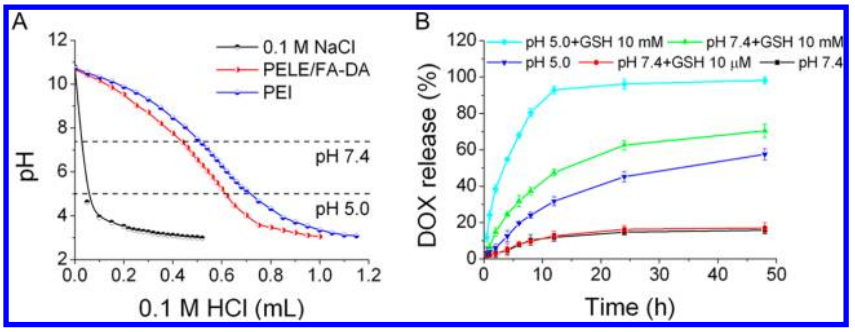

Figure 4. (A) Buffering capacity of PELE/FA-DA obtained by titrating polymer aqueous solution (2 mg/mL) in 0.1 M NaCl aqueous solution (pH 11, adjusted with NaOH) with 0.1 M HCl. PEI was used as the control sample. (B) *In vitro* quantitative DOX release from the PELE/FA-DA micelles. Data are shown as mean ± SD (n = 3).

charge-reversal behavior was observed by the PELE-SA micelles, whose ζ-potentials remained between −20 mV and −15 mV at pH 7.4, pH 6.8, and pH 5.0 (Figure S12A in SI).

To further confirm the pH-dependent charge reversal, the size change of PELE/FA-DA and PELE-SA micelles against time at physiological condition and acidic condition was measured by DLS. At pH 7.4, the size of PELE/FA-DA micelles did not change within 24 h, indicating the high stability of the micelles under physiological condition (Figure 3B). However, the micellar size gradually increased at pH 6.8, and significantly increased at pH 5.0. In acidic condition, the primary amine and secondary amine groups of PEI were partially protonated at pH 6.8 or completely protonated at pH 5.0, and thus the segment was stretched in varying degrees. As a result, the enhanced force caused by shell expansion and electrostatic repulsion of protonated amine groups led to the size increase of micelles. However, there was no significant difference in the particle size of PELE-SA micelles at pH 7.4, pH 6.8, and pH 5.0 (Figure S12B in SI).

To verify the reductive responsiveness of the PELE/FA-DA micelles, their size change against different concentrations of GSH was detected. Notably, fast aggregation was observed for the micelles when 10 mM GSH was treated, in which the micellar size increased from 91 to 295 nm in 2 h, reaching over 600 nm after 24 h (Figure 3C). The aggregates were formed due to the reductive cleavage of the disulfide bond between PLA and PEI, resulting in the shedding of the PEI shells as illustrated in Scheme 1, and a low hydrophilicity/hydrophobicity ratio of mPEG−PLA could not form stable micelles, finally demicellization happened. In contrast, no change in the PELE/FA-DA micellar size was discerned after 24 h incubation with 10 μM GSH which is close to the GSH concentration in physiological conditions.

To further identify the demicellization process induced by GSH, a fluorescence spectroscopy using pyrene as the probe was performed (Figure 3D). Reductive demicellization of the PELE/FA-DA micelles was tested in GSH solutions with four concentrations to characterize the critical concentration of GSH that would trigger the reductive degradation of disulfide bonds in the micelles. The ratio of I_{339}/I_{333}, an index of micelle structures, is dependent on the GSH concentration. At 10 μM or 0.1 mM GSH, the ratio of I_{339}/I_{333} did not change or slightly decreased in 120 min, indicating that such a low GSH concentration can hardly destroy the core−shell structure of the PELE/FA-DA micelles. At 1 mM GSH, the ratio of I_{339}/I_{333} decreased 16.5% after 120 min. When the GSH concentration was increased up to 10 mM, the demicellization of micelles became much faster: the I_{339}/I_{333} ratio dropped 54.4% in 120 min. These results suggest that the PELE/FA-DA micelles are quickly dissociated in a GSH concentration greater than 1 mM, below which they will preserve the core−shell structure.

To demonstrate the demicellization process triggered by both acidic pH and GSH, we observed the change of the micellar morphology with TEM. As shown in Figure 3E, we can find that the PELE/FA-DA micelles without treatment have a spherical shape and a uniform distribution. When the PELE/FA-DA micelles were incubated with 10 mM GSH at pH 5.0, the disassembly of micelles was observed. This finding was due to the fact that the micelles were positively charged in acidic pH, and the PEI segment became unconsolidated, which facilitated GSH penetrating into micelles to fracture the disulfide bond and finally destroy the micelle structure. Therefore, drying the solution led to the formation of random polymeric aggregates (Figure 3F).

As we know, lysosomal escape of NPs is critical for successfully delivering drug. A main advantage of PEI is its buffering capacity, which can facilitate its lysosomal escape.[37] To assess the proton buffering capacity of the PELE/FA-DA, acid−base titration was performed (Figure 4A). The result showed that this terpolymer has a buffering capacity (16.77%) similar to that of PEI (18.69%), indicating that the conjugation of PEI to PELA hardly reduced its buffering capacity. Thus, PELE/FA-DA micelles are able to absorb protons in the endo/lysosomes as the second-stage pH response after charge reversal, leading to an increase in osmotic pressure inside the endo/lysosomes, followed by plasma membrane disruption and micelle release into the cytoplasm.[16]

***In Vitro* Drug Release.** To confirm whether the micelles can rapidly release the encapsulated drug under conditions similar to the tumor microenvironment, *in vitro* drug release from the DOX-loaded PELE/FA-DA micelles was investigated. From Figure S13 in SI, we can find that the DOX fluorescence intensity in the DOX-loaded PELE/FA-DA micelle group was very weak within 2 h at pH 7.4 without adding GSH, whereas it was obviously intensified when adjusting the solution pH value to 5.0 or adding GSH. Besides, the highest DOX fluorescence intensity was detected when both acidic pH and reducing agent were applied. Consistent results were obtained in the quantitative determination of DOX release (Figure 4B). Drug release of the solution at pH 7.4 or adding 10 μM GSH was less than 20% within the experimental time of 48 h, implying that DOX was steadily sequestrated within the micelles during blood circulation (~10 μM GSH). On the contrary, a rapid release of DOX was turned on immediately at pH 5.0 or 10 mM GSH was added. Furthermore, the most rapid release was determined when the dual stimuli were applied simultaneously.

dx.doi.org/10.1021/cm5012718 | *Chem. Mater.* 2014, 26, 4405−4418

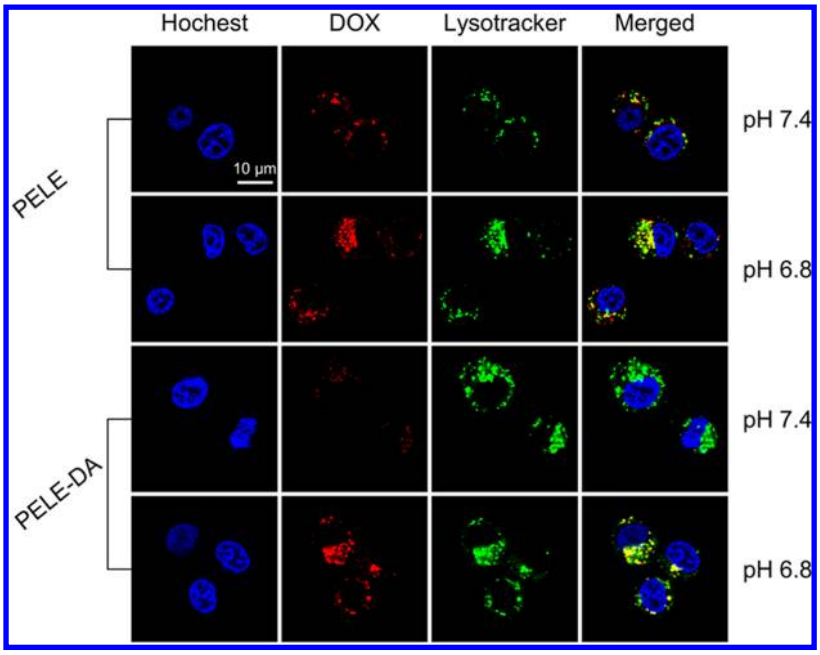

Figure 5. Cellular uptake of DOX-loaded PELE and PELE-DA micelles at pH 7.4 or 6.8 after incubation with HeLa cells for 1 h (DOX-equivalent dose: 5 μg/mL). Nuclei and lysosomes were stained with Hoechst 33342 (blue) and Lysotracker (green), respectively.

When the solution was adjusting to pH 5.0 and 10 mM GSH was added, more than 90% of DOX was released within 12 h. The result indicates that the dual responsive drug-loaded micelles can rapidly release the cargo after lysosomal escape.

FR Surface Expression. Considering the negligible FR levels expressed by mouse mammary tumor 4T1 cells,[38] a continuous culturing of folate (10 pmol/L) was treated with the cells to upregulate the FR expression. Flow cytometry was performed to evaluate the FR surface expression of nontreated 4T1 cells and folate-treated 4T1 cells by indirect immunostaining, and FR-overexpressed human cervix adenocarcinoma HeLa cells were used as positive control.[39] The result showed that the FA-treated 4T1 cells express a much higher level of FR than the nontreated 4T1 cells (Figure S14 in SI), indicating a successful upregulation of FR expression. Thus, the FR-upregulated 4T1 cells were used for the following *in vitro* and *in vivo* studies.

Cytocompatibility Assay. As a drug carrier, good cytocompatibility of the vector itself was essential for clinical applications. Cytocompatibility assay of blank micelles was estimated against mouse fibroblast NIH 3T3 cells, HeLa cells, and 4T1 cells at pH 7.4 and 6.8 via Alarmar blue (AB) assay. The results against the three kinds of cells at pH 7.4 showed that the cell viabilities were still above 90% when the concentration of PELE-DA or PELE/FA-DA micelles was as high as 250 μg/mL (Figure S15 in SI). On the contrary, the PELE micelles showed serious cytotoxicity. Therefore, the charge-reversal groups modified on PEI have the ability to reduce nonspecific uptake by normal cells and in turn reduce toxicity. At pH 6.8, the PELE-DA and PELE/FA-DA micelles possessed similar cytotoxicity compared with PELE micelles (Figure S16 in SI). This is because the amides between PEI and DA quickly hydrolyzed in acidic conditions, and the two micelles immediately deshielded DA groups and turned to positively charged PELE and PELE/FA micelles, respectively (Figure 2A and Figure 3A). This selective acidic cytotoxicity of charge-reversal micelles is not only conducive to cancer therapy but also safe to the body. The images of live/dead staining for NIH 3T3 cells are in line with the AB assay (Figure S17 and Figure S18 in SI).

***In Vitro* Cellular Uptake and Subcellular Localization.** Previous studies reported that negatively charged NPs inhibited cellular uptake in a remarkable manner.[40,41] Thus, reversing the surface charge of negatively charged micelles would enhance the cellular uptake. To verify whether the charge-reversal micelles can be more efficiently internalized by cancer cells at the acidic pH, we compared the cellular uptake behaviors of various formulations at pHs 7.4 and 6.8. FR-negative human lung epithelial carcinoma A549 cells[42] were incubated with free DOX or DOX-loaded micelles at each pH for 3 h, and the cellular uptake was observed with the fluorescence microscope. As shown in Figure S19 in SI, the charge-reversal micelles were remarkably internalized at pH 6.8, which were rarely observed in the cells incubated with the same micelles at pH 7.4. In contrast, the internalization of the neutral PECL micelles by A549 cells was not significantly affected by pH, where very similar fluorescence intensity was observed in the cells treated with the micelles at pH 7.4 and 6.8. A slight increase of DOX fluorescence was observed for A549 cells treated with free DOX and DOX-loaded PELE micelles at pH 6.8 compared to that at pH 7.4, which was attributed to the increased solubility of DOX and PEI at acidic pH upon protonation of amine groups. Moreover, no obvious different fluorescence intensity was observed in the cells incubated with PELE/FA-DA and PELE-DA micelles at both pH conditions, indicating that folate could not target FR negative cells. The quantitative flow cytometric analyses further proved the pH-dependent endocytosis of the charge-reversal micelles by HeLa cells (Figure S20 in SI). After incubation for 3 h, the internalizations of the charge-reversal micelles were significantly enhanced at pH 6.8, which was similar to the results of Figure S19 in SI, and the only difference was that the FA-attached micelles were internalized more than FA-free micelles, indicating that PELE/FA-DA micelles selectively target the FR-overexpressed cancer cells.

Confocal laser scanning microscopy (CLSM) analysis was performed for HeLa cells to evaluate the charge reversal as well.

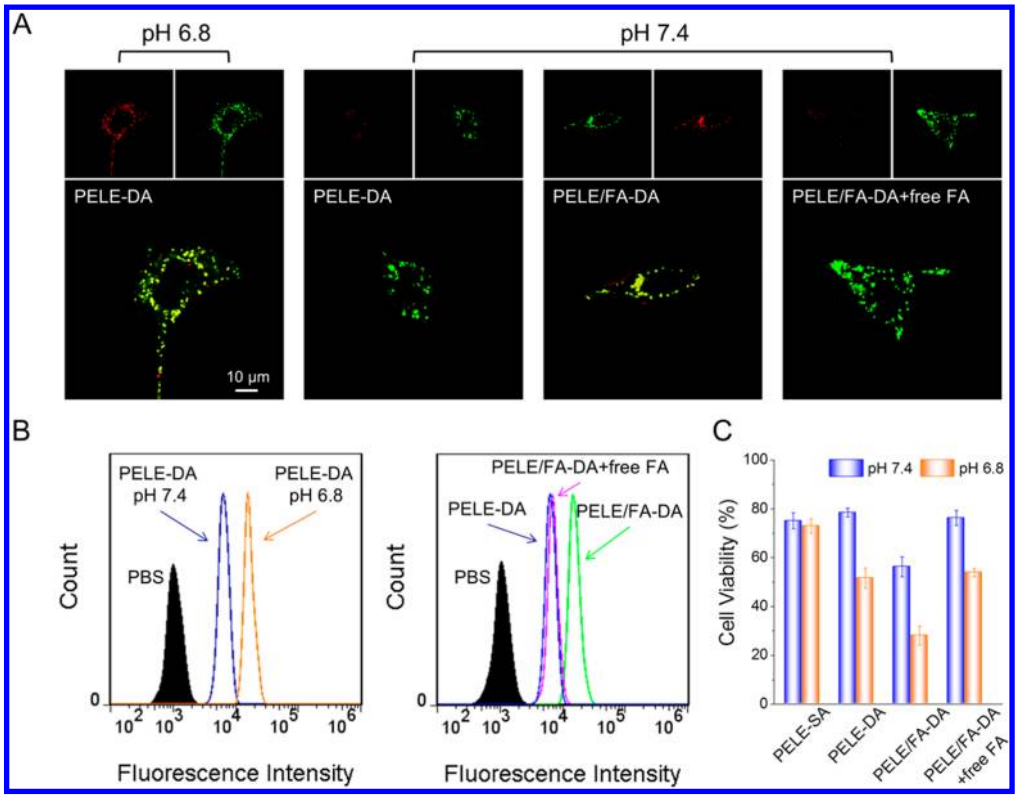

Figure 6. (A) CLSM images and (B) flow cytometry analysis of DOX-loaded PELE-DA at pH 7.4 or pH 6.8, and PELE/FA-DA or PELE/FA-DA micelles with a blocking dose of free FA at pH 7.4 after incubation with 4T1 cells for 1 h (DOX-equivalent dose: 5 μg/mL). Lysosomes were stained with Lysotracker (green). (C) Viability of 4T1 cells after incubation with various DOX-loaded micelles at pH 7.4 or pH 6.8 for 24 h (DOX-equivalent dose: 10 μg/mL) (n = 4).

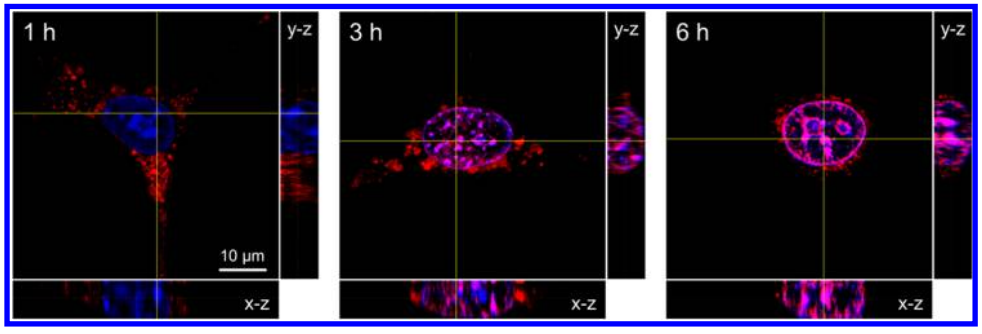

Figure 7. Z-stack images of the DOX-loaded PELE/FA-DA micelles uptake and drug release process in 4T1 cells at pH 6.8 for 1, 3, and 6 h (DOX-equivalent dose: 5 μg/mL). Nuclei were stained with DAPI (blue).

The cells were incubated with DOX-loaded PELE and PELE-DA micelles for 1 h; similar internalization was observed for PELE micelles at pH 7.4 and 6.8, while intensified fluorescence was detected for PELE-DA micelles at acidic pH (Figure 5). Both the two classes of micelles were located in the lysosomes, demonstrating that drug release did not occur in 1 h.

To simultaneously investigate the charge-reversal internalization and FR-mediated endocytosis, CLSM, and flow cytometry were performed after the DOX-loaded micelles were incubated with 4T1 cells for 1 h. Significantly distinct cellular uptake was observed for the DOX-loaded PELE-DA micelles at different pH values. At pH 6.8, the DOX fluorescence was internalized to a remarkable extent, whereas at pH 7.4, little internalization of PELE-DA micelles occurred (Figure 6A and B). In contrast, no different internalization was observed at pH 7.4 or 6.8 when the PELE-SA micelles were incubated with 4T1 cells (Figure S21 in SI). Taken together, it can be concluded that the charge-reversal micelles could significantly enhance cellular internalization at slightly acidic pH value against A549, HeLa, and 4T1 cells. Moreover, the cellular uptake of DOX-loaded PELE-DA, PELE/FA-DA, or PELE/FA-DA micelles with a blocking dose of free FA at pH 7.4 showed that FA-attached micelles internalized more obviously than FA-free micelles or FA-blocking micelles (Figure 6A and B). The result evidenced that folate conjugation could indeed increase the cellular uptake of micelles by FR-upregulated 4T1 cells even if they do not express FR levels as high as HeLa cells (Figure S14 in SI). Besides, as shown in Figure S20 (in SI) and Figure 6B, the flow cytometric analyses quantitatively showed that there were no apparent differences in cellular uptake of PELE/FA-DA micelles at pH 7.4 and PELE-DA micelles at pH 6.8, which proved that the extent of enhanced uptake by folate targeting and charge reversal are nearly the same. However, the HeLa cells and 4T1 cells treated

dx.doi.org/10.1021/cm5012718 | Chem. Mater. 2014, 26, 4405−4418

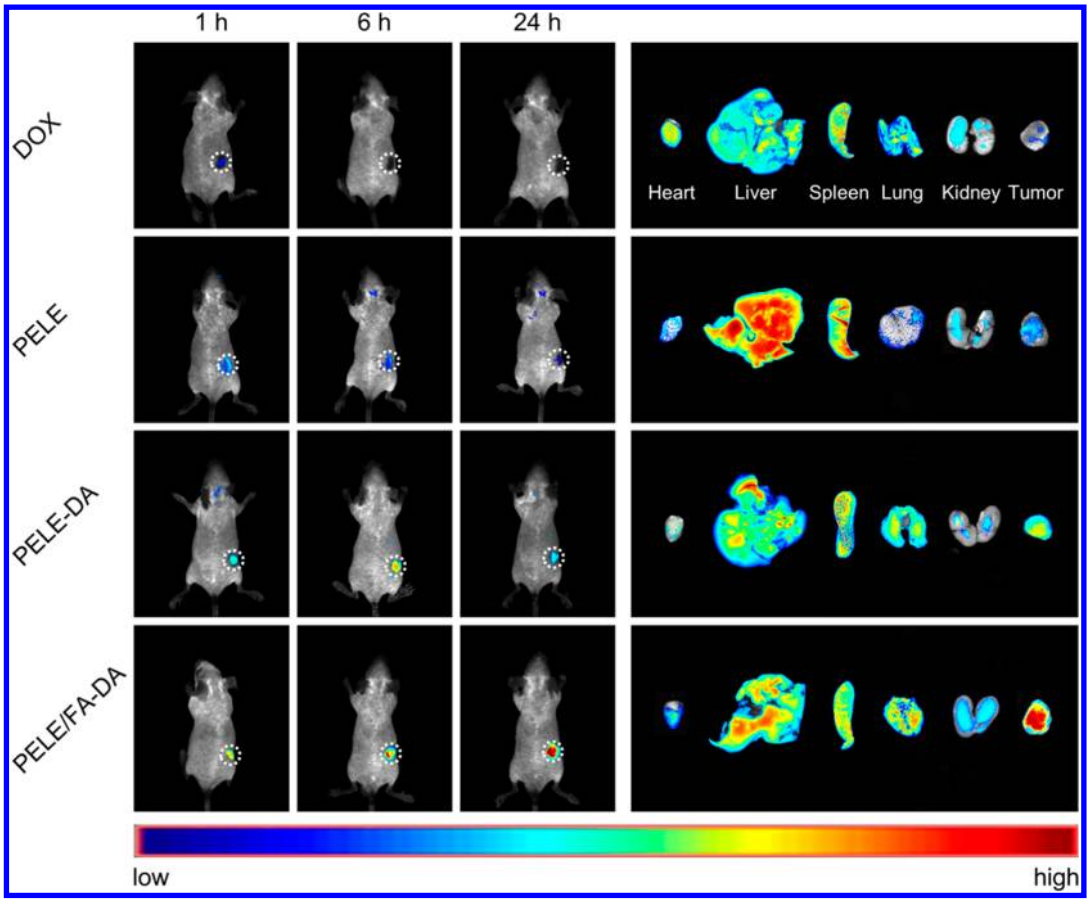

Figure 8. *In vivo* DOX fluorescence images of free DOX and DOX-loaded micelles after tail-vein injection into male nude mice bearing the 4T1 xenograft (dose: 5 mg DOX per kg body weight), and *ex vivo* DOX distribution in isolated tissues at 24 h postinjection.

with PELE/FA-DA micelles at pH 6.8 possessed the highest fluorescence. Therefore, folate targeting and charge reversal are synergistic to enhance cellular uptake.

To demonstrate whether the loaded DOX can be efficiently released to the nucleus after the drug-loaded micelles are internalized by cancer cells, we incubated HeLa cells with different DOX formulations at pH 6.8 for 3 h, and the cells were subjected to CLSM observations. As shown in Figure S22 in SI, HeLa cells treated with the charge-reversal micelles presented strong red fluorescence in the nuclei, suggesting the successful nuclear delivery of DOX from the micelles. The rapid release of DOX from these micelles inside cells was in good agreement with our anticipation in Scheme 1. In contrast, PECL micelles showed very weak fluorescence in the cytoplasm and seemed to be entrapped in the lysosomes.

To prove that the released DOX from the micelles is exactly inside the nucleus instead of on the surface, we incubated 4T1 cells with DOX-loaded PELE/FA-DA micelles at pH 6.8 for 1, 3, and 6 h for observation of Z-stack confocal images. The images revealed that the micelles were distributed in the cytoplasm at 1 h, partial drug release to the nucleus occurred at 3 h; finally, almost all of DOX entered into the nucleus at 6 h (Figure 7).

The Effect of pH Value on Cytotoxicity. To verify the feasibility of the charge-reversal micelles for cancer therapy, we tested the cytotoxicity of different DOX formulations against HeLa cells at pH 7.4 and 6.8 using an AB assay. The DOX-loaded PELE-DA and PELE/FA-DA micelles showed significantly enhanced cytotoxicity at pH 6.8 relative to that at pH 7.4 (Figure S23 in SI). Moreover, PELE/FA-DA micelles revealed even higher cytotoxicity than free DOX at pH 6.8, which can be attributed to the higher cellular uptake exhibited by the FA-attached micelles due to FR-mediated endocytosis. The IC_{50} value of free DOX at pH 7.4 or 6.8 has no obvious difference, indicating that the slightly acidic condition did not affect the cytotoxicity of DOX.[43] Consistent results were obtained by the neutral PECL micelles, which exhibited similar cytotoxicity at the two conditions.

The pH-dependent cytotoxicity of DOX formulations were also evaluated against 4T1 cells. The AB assay further evidenced the higher toxicity of charge-reversal micelles at acidic pH relative to that at neutral conditions (Figure 6C). Not surprisingly, there's no real distinction of the cell viabilities between pH 7.4 and pH 6.8 for the PELE-SA group. Moreover, FA-attached micelles induced more cell death than FA-free or FA-blocking micelles at both pH values, which was caused by the higher uptake of FA-attached micelles (Figure 6).

***In Vivo* and *ex Vivo* DOX Fluorescence Imaging.** To directly visualize the distribution of DOX *in vivo*, we injected various DOX formulations to 4T1 tumor-bearing nude mice, and then monitored the DOX fluorescence in tumors at different time intervals by Maestro in-Vivo Imaging System. Figure 8 shows that strong DOX fluorescence was observed in tumor for charge-reversal micelles after 1 h, as time elapsed, tumor fluorescence in the PELE/FA-DA treated mouse was notably higher than in the PELE-DA treated group. Nevertheless, the fluorescence intensity of free DOX and PELE groups decreased significantly 1 h later. The *in vivo* imaging

dx.doi.org/10.1021/cm5012718 | *Chem. Mater.* 2014, 26, 4405−4418

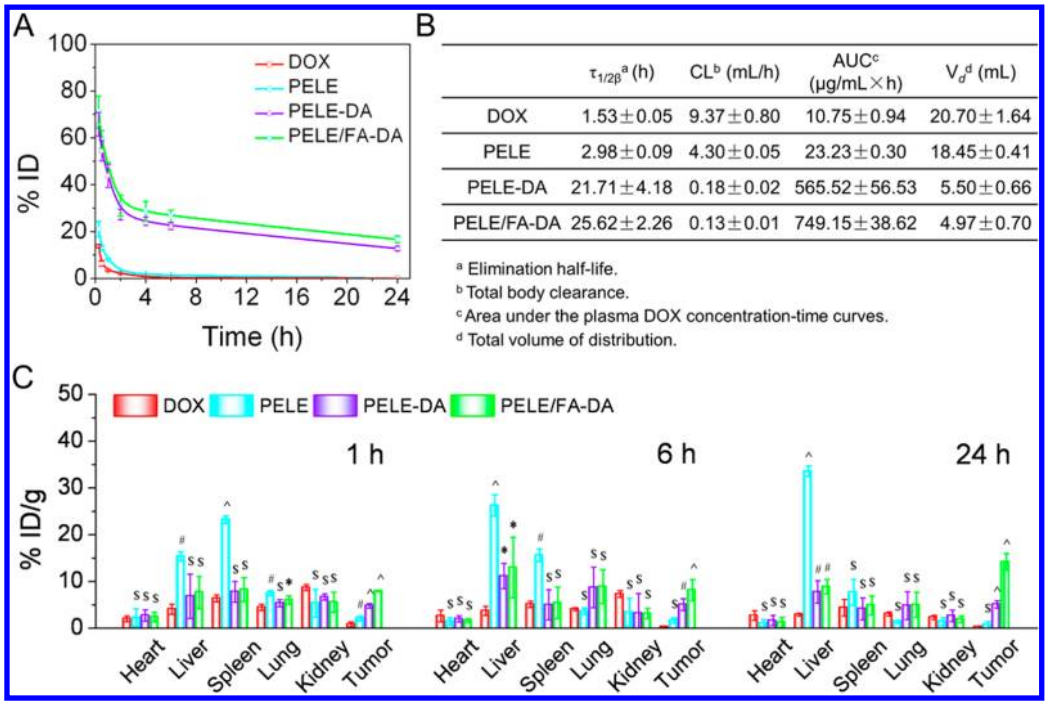

	$\tau_{1/2\beta}$[a] (h)	CL[b] (mL/h)	AUC[c] (μg/mL×h)	V_d[d] (mL)
DOX	1.53±0.05	9.37±0.80	10.75±0.94	20.70±1.64
PELE	2.98±0.09	4.30±0.05	23.23±0.30	18.45±0.41
PELE-DA	21.71±4.18	0.18±0.02	565.52±56.53	5.50±0.66
PELE/FA-DA	25.62±2.26	0.13±0.01	749.15±38.62	4.97±0.70

[a] Elimination half-life.
[b] Total body clearance.
[c] Area under the plasma DOX concentration-time curves.
[d] Total volume of distribution.

Figure 9. (A) Pharmacokinetic profiles of total DOX after tail vein injection of various DOX formulations (dose: 5 mg DOX per kg body weight) (n = 3). (B) Pharmacokinetic parameters of various DOX forumulations. (C) Biodistribution of DOX for various therapeutic micelle formulations after intravenous injection at a dose of 5 mg/kg (n = 3). $, not significant; *, $P < 0.05$; #, $P < 0.01$; ^, $P < 0.001$, as compared with free DOX at the same time point (one way ANOVA using SPSS, 17.0).

indicated that PELE/FA-DA micelles have excellent targeting efficiency and accumulates continuously in tumors compared to other groups. At 24 h postinjection, we excised normal tissues and tumor from the sacrificed mice to directly observe the DOX fluorescence distribution. *Ex vivo* imaging showed that charge-reversal micelles significantly reduced liver distribution while tumor accumulation increased compared with PELE micelles (Figure 8). Due to the fast elimination of free DOX, it possessed the weakest tumor fluorescence among all groups.

Pharmacokinetics and Biodistribution *in Vivo*. Surface charge plays a key role in nonspecific cellular uptake and protein absorption in blood circulation.[44] Particles with a positively charged surface are expected to exhibit a rapid blood clearance phase with a large dose accumulation in liver and spleen.[45] Therefore, reducing surface charge can decrease liver and splenic uptake, and the negatively charged surface can block the electrostatic and hydrophobic interactions that help opsonins bind to particle surfaces.[46] To demonstrate this quantitatively, we treated Balb/c mice with a single intravenous injection of different DOX formulations, collected plasma and tissues at different time intervals, and determined the level of DOX by fluorescence spectroscopy. From the blood clearance curves (Figure 9A), and the pharmacokinetic parameters obtained by fitting the blood DOX concentration versus time using a two-compartment model (Figure 9B), we find that the elimination of DOX from the blood was significantly slower when it was loaded with the charge-reversal micelles compared to the free DOX and PELE micelles. Besides, similar to *ex vivo* imaging in Figure 8, the result of DOX distribution in tissues indicated that charge-reversal micelles with negative charge in blood circulation and positive charge in tumor displayed less RES uptake and more tumor accumulation than PELE micelles which were always positively charged (Figure 9C). Although both the two charge-reversal micelles have a high accumulation in tumor, the actively targeting effect still plays an important role as the accumulation of FA-attached micelles increased in tumor but decreased in normal tissues compared to that of FA-free micelles.

***In Vivo* Antitumor Effect.** To further explore the potential of the charge-reversal micelles for *in vivo* cancer therapy, the antitumor effect and systemic toxicity of the various formulations injected into 4T1 tumor-bearing Balb/c mice were examined. Based on the tumor volume (Figure 10A), the charge-reversal micelles showed a comparable tumor growth suppression in contrast to free DOX, especially the PELE/FA-DA micelles, which exhibited the highest tumor growth inhibition efficacy among all of these formulations. The inhibition rate of tumor growth (IR) was calculated on the basis of the tumor volume at day 21 (Figure S24 in SI). The IR of the PELE/FA-DA micelles was calculated to be 90.51% ± 2.96%, which was 1.21-fold and 1.56-fold of PELE-DA and PELE micelles, respectively, while free DOX possessed the lowest IR compared to DOX-loaded micelles. Figure 10B shows the variation of body weight of the 4T1 tumor-bearing Balb/c mice with time. Compared to the initial body weights of mice, a slight body weight increase was observed after the injection of the DOX-loaded charge-reversal micelles, while mice treated with free DOX and DOX-loaded PELE micelles showed significant weight loss. Moreover, the survival rate of mice also demonstrated that the charge-reversal micelles possessed better safety for the body (Figure 10C).

In situ histological and immunohistochemical studies were supportive of the excellent therapeutic effect of the actively targeted charged-reversal micelles. The fewest tumor cells and the highest level of cell apoptosis were shown in H&E staining and TUNEL analysis in the PELE/FA-DA group (Figure 10D). Moreover, the apoptotic rate (AR) was calculated on the basis of TUNEL analysis by Image-Pro Plus 6.0 (Figure 10E).

dx.doi.org/10.1021/cm5012718 | *Chem. Mater.* 2014, 26, 4405−4418

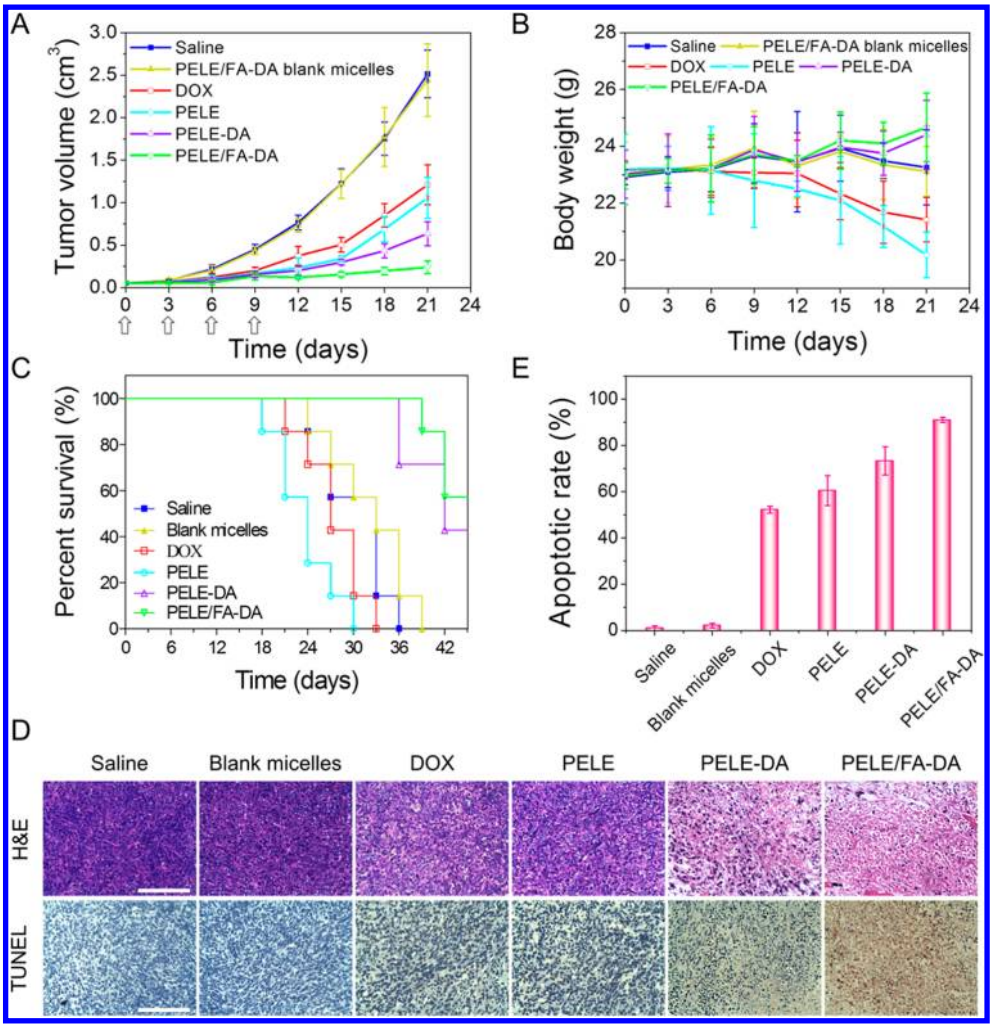

Figure 10. (A) Tumor growth inhibition, (B) weight changes, and (C) survival curves of Balb/c mice (n = 7) bearing 4T1 tumor after tail vein injection of different formulations (dose: 5 mg DOX per kg body weight per injection for DOX-loaded formulations; injection was performed every 3 days). (D) Ex vivo histological analyses of tumor sections (21 days after the first treatment). In H&E staining, nuclei are stained blue, and extracellular matrix and cytoplasm are stained red. In TUNEL analysis, blue and brown stains indicate normal and apoptotic cells, respectively. Scale bars in (D) represent 100 μm. (E) Apoptotic rate calculated by Image-Pro Plus 6.0 in TUNEL analysis. The values in (A), (B), and (E) are mean ± SD; $, not significant; #, $P < 0.01$; ^, $P < 0.001$, as compared with saline group (one way ANOVA using SPSS, 17.0).

Interestingly, we found that the AR of each group was quite similar to the respective IR (Figure S24 in SI), indicating that the DOX-loaded PELE/FA-DA micelles presented the best antitumor effect whether from the point of inhibiting tumor growth or causing cell apoptosis.

CONCLUSION

In summary, we have demonstrated a novel dual-responsive polymer micelle for target-cell-specific anticancer drug delivery. This micelle with originally negatively charged surface in blood can significantly prolong the circulation time. Once the micelle accumulates at the tumor site by the EPR effect, it represents an ultrasensitive negative-to-positive charge reversal in response to the acidic pH value, and thus it can be significantly internalized by cancer cells through electronic interaction and FR-mediated endocytosis, escape from the lysosomes via a proton sponge effect, and deshield the PEI shells triggered by excess intracellular GSH and finally ship the therapeutic agent to the nucleus to ensure high cytotoxicity to the target cell. We expect that this nanomedicine can provide a promising platform for effective cancer therapy.

ASSOCIATED CONTENT

Supporting Information

Syntheses procedures of polymers. Additional figures including Figure S1−S24 and Tables S1−S2 as described in the text. This material is available free of charge via the Internet at http://pubs.acs.org.

AUTHOR INFORMATION

Corresponding Author

*E-mail: shaobingzhou@swjtu.cn; shaobingzhou@hotmail.com.

Notes

The authors declare no competing financial interest.

ACKNOWLEDGMENTS

This work was partially supported by the National Basic Research Program of China (973 Program, 2012CB933600), National Natural Science Foundation of China (Nos. 30970723, 51173150, 51373138), Research Fund for the Doctoral Program of Higher Education of China (20120184110029), and Construction Program for Innovative Research Team of University in Sichuan Province (14TD0050).

REFERENCES

(1) Friesen, C.; Uhl, M.; Pannicke, U.; Schwarz, K.; Miltner, E.; Debatin, K. M. *Mol. Biol. Cell* **2008**, *19*, 3283−3289.
(2) Fuertes, M. A.; Castilla, J.; Alonso, C.; Pérez, J. M. *Recent Res. Devel. Mol. Pharmacol.* **2002**, *1*, 37−51.
(3) Peer, D.; Karp, J. M.; Hong, S.; Farokhzad, O. C.; Margalit, R.; Langer, R. *Nat. Nanotechnol.* **2007**, *2*, 751−760.
(4) Maeda, H.; Nakamura, H.; Fang, J. *Adv. Drug Deliverery Rev.* **2012**, *65*, 71−79.
(5) Yamamoto, Y.; Nagasaki, Y.; Kato, Y.; Sugiyama, Y.; Kataoka, K. *J. Controlled Release* **2001**, *77*, 27−38.
(6) Oupicky, D.; Ogris, M.; Howard, K. A.; Dash, P. R.; Ulbrich, K.; Seymour, L. W. *Mol. Ther.* **2002**, *5*, 463−472.
(7) Allen, T. M. *Nat. Rev. Cancer* **2002**, *2*, 750−763.
(8) Dong, H. F.; Lei, J. P.; Ju, H. X.; Zhi, F.; Wang, H.; Guo, W. J.; Zhu, Z.; Yan, F. *Angew. Chem., Int. Ed.* **2012**, *51*, 4607−4612.
(9) Fan, N. C.; Cheng, F. Y.; Ho, J. A. A.; Yeh, C. S. *Angew. Chem., Int. Ed.* **2012**, *51*, 8806−8810.
(10) Guo, X.; Shi, C. L.; Wang, J.; Di, S. B.; Zhou, S. B. *Biomaterials* **2013**, *34*, 4544−4554.
(11) Ahmed, E.; Morton, S. W.; Hammond, P. T.; Swager, T. M. *Adv. Mater.* **2013**, *25*, 4504−4510.
(12) Hubbell, J. A. *Science* **2003**, *300*, 595−596.
(13) Liu, X. S.; Chen, Y. J.; Li, H.; Huang, N.; Jin, Q.; Ren, K. F.; Ji, J. *ACS Nano* **2013**, *7*, 6244−6257.
(14) Duan, X. P.; Xiao, J. S.; Yin, Q.; Zhang, Z. W.; Yu, H. J.; Mao, S. R.; Li, Y. P. *ACS Nano* **2013**, *7*, 5858−5869.
(15) Johnson, R. P.; Jeong, Y. I.; Choi, E.; Chung, C. W.; Kang, D. H.; Oh, S. O.; Suh, H.; Kim, I. *Adv. Funct. Mater.* **2012**, *22*, 1058−1068.
(16) Mo, R.; Sun, Q.; Xue, J. W.; Li, N.; Li, W. Y.; Zhang, C.; Ping, Q. N. *Adv. Mater.* **2012**, *24*, 3659−3665.
(17) Du, J. Z.; Du, X. J.; Mao, C. Q.; Wang, J. *J. Am. Chem. Soc.* **2011**, *133*, 17560−17563.
(18) Zhou, Z. X.; Shen, Y. Q.; Tang, J. B.; Fan, M. H.; Van Kirk, E. A.; Murdoch, W. J.; Radosz, M. *Adv. Funct. Mater.* **2009**, *19*, 3580−3589.
(19) Romberg, B.; Hennink, W. E.; Storm, G. *Pharm. Res.* **2008**, *25*, 55−71.
(20) Wang, X. Y.; Cai, X. P.; Hu, J. J.; Shao, N. M.; Wang, F.; Zhang, Q.; Xiao, J. R.; Cheng, Y. Y. *J. Am. Chem. Soc.* **2013**, *135*, 9805−9810.
(21) Zhang, J.; Yuan, Z. F.; Wang, Y.; Chen, W. H.; Luo, G. F.; Cheng, S. X.; Zhuo, R. X.; Zhang, X. Z. *J. Am. Chem. Soc.* **2013**, *135*, 5068−5073.
(22) Wei, H.; Volpatti, L. R.; Sellers, D. L.; Maris, D. O.; Andrews, I. W.; Hemphill, A. S.; Chan, L. W.; Chu, D. S.; Horner, P. J.; Pun, S. H. *Angew. Chem., Int. Ed.* **2013**, *52*, 5377−5381.
(23) Torchilin, V. P. *Pharm. Res.* **2007**, *24*, 1−16.
(24) Kakizawa, Y.; Kataoka, K. *Adv. Drug Delivery Rev.* **2002**, *54*, 203−222.
(25) Kwon, G. S.; Okano, T. *Adv. Drug Delivery Rev.* **1996**, *21*, 107−116.
(26) Bausinger, R.; von Gersdorff, K.; Braeckmans, K.; Ogris, M.; Wagner, E.; Bräuchle, C.; Zumbusch, A. *Angew. Chem.* **2006**, *118*, 1598−1602.
(27) Suh, J.; Wirtz, D.; Hanes, J. *Proc. Natl. Acad. Sci. U.S.A.* **2003**, *100*, 3878−3882.
(28) Godbey, W. T.; Wu, K. K.; Mikos, A. G. *Proc. Natl. Acad. Sci. U.S.A.* **1999**, *96*, 5177−5181.
(29) Kluger, R.; Lam, C. H. *J. Am. Chem. Soc.* **1978**, *100*, 2191−2197.
(30) Xu, P. S.; Van Kirk, E. A.; Zhan, Y. H.; Murdoch, W. J.; Radosz, M.; Shen, Y. Q. *Angew. Chem., Int. Ed.* **2007**, *46*, 4999−5002.
(31) Reddy, J. A.; Xu, L. C.; Parker, N.; Vetzel, M.; Leamon, C. P. *J. Nucl. Med.* **2004**, *45*, 857−866.
(32) Rosenholm, J. M.; Meinander, A.; Peuhu, E.; Niemi, R.; Eriksson, J. E.; Sahlgren, C.; Lindén, M. *ACS Nano* **2008**, *3*, 197−206.
(33) Zhu, S. J.; Hong, M. H.; Tang, G. T.; Qian, L. L.; Lin, J. Y.; Jiang, Y. Y.; Pei, Y. Y. *Biomaterials* **2010**, *31*, 1360−1371.
(34) Fonge, H.; Huang, H.; Scollard, D.; Reilly, R. M.; Allen, C. *J. Controlled Release* **2012**, *157*, 366−374.
(35) Davis, M. E.; Chen, Z.; Shin, D. M. *Nat. Rev. Drug Discovery* **2008**, *7*, 771−782.
(36) Du, J. Z.; Sun, T. M.; Song, W. J.; Wu, J.; Wang, J. *Angew. Chem.* **2010**, *122*, 3703−3708.
(37) Boussif, O.; Lezoualc', H. F.; Zanta, M. A.; Mergny, M. D.; Scherman, D.; Demeneix, B.; Behr, J. *Proc. Natl. Acad. Sci. U.S.A.* **1995**, *92*, 7297−7301.
(38) Parker, N.; Turk, M. J.; Westrick, E.; Lewis, J. D.; Low, P. S.; Leamon, C. P. *Anal. Biochem.* **2005**, *338*, 284−293.
(39) Chan, S. Y.; Empig, C. J.; Welte, F. J.; Speck, R. F.; Schmaljohn, A.; Kreisberg, J. F.; Goldsmith, M. A. *Cell* **2001**, *106*, 117−126.
(40) Gratton, S. E.; Ropp, P. A.; Pohlhaus, P. D.; Luft, J. C.; Madden, V. J.; Napier, M. E.; DeSimone, J. M. *Proc. Natl. Acad. Sci. U.S.A.* **2008**, *105*, 11613−11618.
(41) Cho, E. C.; Xie, J.; Wurm, P. A.; Xia, Y. *Nano Lett.* **2009**, *9*, 1080−1084.
(42) Parker, N.; Turk, M. J.; Westrick, E.; Lewis, J. D.; Low, P. S.; Leamon, C. P. *Anal. Biochem.* **2005**, *338*, 284−293.
(43) Kim, D.; Lee, E. S.; Oh, K. T.; Gao, Z. G.; Bae, Y. H. *Small* **2008**, *4*, 2043−2050.
(44) Wang, J.; Byrne, J. D.; Napier, M. E.; DeSimone, J. M. *Small* **2011**, *7*, 1919−1931.
(45) Li, S.; Huang, L. *Mol. Pharmaceutics* **2008**, *5*, 496−504.
(46) Owens, D. E., III; Peppas, N. A. *Int. J. Pharm.* **2006**, *307*, 93−102.